

Highlights

Global-Local Dynamic Feature Alignment Network for Person Re-Identification

Zhangqiang Ming, Yong Yang, Xiaoyong Wei, Jianrong Yan, Xiangkun Wang, Fengjie Wang, Min Zhu

- We propose a new method name LSA that achieves dynamic alignment of local features by setting sliding windows for their local stripes
- LSA can effectively suppress spatially misalignment and the noises from unshared regions.
- LSA does not require the additional auxiliary pose information.
- We design a Global-Local Dynamic Feature Alignment Network (GLDFA-Net) framework, which contains two branches, global and local.
- LSA is introduced into the local branch of GLDFA-Net to guide the computation of the distance metric.

Global-Local Dynamic Feature Alignment Network for Person Re-Identification

Zhangqiang Ming, Yong Yang, Xiaoyong Wei, Jianrong Yan, Xiangkun Wang, Fengjie Wang and Min Zhu*

College of Computer Science, Sichuan University, Chengdu, 610065, China

ARTICLE INFO

Keywords:

Person Re-Identification
Feature Learning
GLDFA-Net
Local Sliding Alignment

ABSTRACT

The misalignment of human images caused by pedestrian detection bounding box errors or partial occlusions is one of the main challenges in person Re-Identification (Re-ID) tasks. Previous local-based methods mainly focus on learning local features in predefined semantic regions of pedestrians, but usually use local hard alignment methods or introduce auxiliary information such as key human pose points to match local features. These methods are often not applicable when large scene differences are encountered. Targeting to solve these problems, we propose a simple and efficient Local Sliding Alignment (LSA) strategy to dynamically align the local features of two images by setting a sliding window on the local stripes of the pedestrian. LSA can effectively suppress spatial misalignment and does not need to introduce extra supervision information. Then, we design a Global-Local Dynamic Feature Alignment Network (GLDFA-Net) framework, which contains both global and local branches. We introduce LSA into the local branch of GLDFA-Net to guide the computation of distance metrics, which can further improve the accuracy of the testing phase. Evaluation experiments on several mainstream evaluation datasets including Market-1501, DukeMTMC-reID, and CUHK03 show that our method has competitive accuracy over the several state-of-the-art person Re-ID methods. Additionally, it achieves 86.1% mAP and 94.8% Rank-1 accuracy on Market1501.

1. Introduction

Person Re-Identification (Re-ID) is a challenging task in the field of computer vision, aiming to determine whether a person capture by different cameras or person images from different video clips of the same camera is the same person. However, due to the complexity of realistic scenarios, person Re-ID still faces many challenges, like person detection bounding box errors, pose misalignments and occlusion, as shown in Figure 1, making it difficult for people to identify a specific person from large gallery collections. To address these challenges, most prior works have a focus on learning global features of pedestrians using Convolutional Neural Networks (CNN), the idea of which can be summarized mainly as representational learning and distance metric learning[24]. Traditional representation learning methods aim to learn the rigid and invariant features [3, 53–55], and most distance metric learning methods aim to reduce the distance of the same person [5, 11, 31, 32]. However, all these methods learn features from the entire image, and contain only the coarse-grained global information of the pedestrian, while ignoring local key details.

To better learn local features, some methods [10, 34, 36, 39] use horizontal stripes or grids to extract local features of person body parts, but such methods require pre-adjust pedestrian alignment to obtain good performance. Some researchers [2, 4, 17, 21] also present attentional mechanisms to complement discriminative features while bringing in extra background attention, which affects the final feature representation of the person. There are also some works [9, 12, 33, 49, 50, 58] using human pose points obtain by human pose estimation models to match different body parts or align key pose points, but training such models requires a huge amount of label data, and additional computational resources are consumed. Alternatively, some researchers [12, 18, 24, 33, 41, 42, 44, 51] combine global and local features to enhance the final pedestrian diversified feature representation. In general, these methods either require the introduction of pedestrian pose to assist in the alignment of local features, but require additional computational resources; or they use local hard alignment to match pedestrian local features, but it is difficult to obtain high person

*Corresponding author

✉ mingzhangqiang@stu.scu.edu.cn (Z. Ming); yangyong@stu.scu.edu.cn (Y. Yang); cswei@scu.edu.cn (X. Wei); zhumin@scu.edu.cn (M. Zhu)

ORCID(s): 0000-0003-1616-8054 (Z. Ming); 0000-0002-5664-1558 (M. Zhu)

Re-ID accuracy with hard alignment when encountering large scene differences such as pedestrian pose changes, pedestrian detection bounding box errors and partial occlusions.

In this paper, we propose a simple and efficient Local Sliding Alignment (LSA) strategy. We first divide the original image into horizontal stripes, and the local features are more focused on finer discriminative features in each strip. LSA achieves dynamic alignment of local stripes by setting sliding windows for local stripes of pedestrians and calculating the shortest alignment distance of local stripes within each sliding window. Compared with the methods of local hard alignment and pose guided alignment, LSA can effectively alleviate the problem of unaligned images due to detection of bounding box errors and partial occlusions and does not require the introduction of additional supervision information. Then, to explore global and local information, we design a Global-Local Dynamic Feature Alignment Network (GLDFA-Net) framework for the person Re-ID task, which contains both global and local branches that learn feature representations at different granularities. We introduce LSA into the local branch of GLDFA-Net to guide the computation of distance metrics. LSA is not only designed to be simple and efficient but also can effectively improve the accuracy of the model. More specifically, in the training phase, we use LSA to calculate the local alignment distances and combine them with the global distances, together as the sample distance for triplet loss. LSA can shorten the distance of samples with the same ID, thus effectively mining hard samples and guiding the model to learn more discriminative features. In the inference stage, we use LSA to calculate the local alignment distance for similarity measurement, which can further improve the accuracy of person matching. Compared with previous local-based methods, our method is an end-to-end learning process with a simple and efficient network structure, requires only dividing horizontal stripes as local features, and the LSA algorithm is easy to implement. Experiments show that our method performs better on multiple mainstream Re-ID datasets.



Fig. 1: Example images of three persons from Market1501 (first row) and DukeMTMC-reID (second row), respectively. From left to right, the challenging problems of Re-ID are shown in sequence: (a) detecting bounding box errors, (b) large posture changes, (c) partial occlusion.

In summary, the main contributions of this article are summarized as follows:

- We propose a new method name LSA that achieves dynamic alignment of local features by setting sliding windows for their local stripes and calculating the shortest alignment distance of the stripes within the corresponding sliding windows. LSA can effectively suppress spatially misalignment and the noises from unshared regions, and does not require the additional auxiliary pose information.
- We design a Global-Local Dynamic Feature Alignment Network (GLDFA-Net) framework, which contains two branches, global and local. We introduce LSA into the local branch of GLDFA-Net to guide the computation of the distance metric, which can further improve the accuracy of the testing phase.
- The experiments show that our method achieves significant improvements in Rank-1 accuracy and mAP on the Market1501 [52], DukeMTMCReID [56] ,and CUHK03 [15] datasets.

2. Related Works

In this section, we will review some work closely related to this paper, including methods based on deep feature learning and methods based on Local features alignments.

2.1. Deep Feature Learning based Person Re-ID

In recent years, with the rapid development of deep learning, deep learning techniques have been widely used in person Re-ID tasks, and have achieved high retrieval accuracy [31, 32, 53, 55]. Compared with traditional methods, deep neural networks can automatically learn global discriminative features, and only a simple metric function is needed to determine the similarity of two pedestrian images. Current deep learning-based person Re-ID methods can be categorized into two types [24, 44], i.e., representation learning methods and distance metric learning methods. Representation learning methods [3, 19, 53–55] aim to learn the powerful and distinguishing features of pedestrian images. Zheng et al. [53, 55] regard the training process of person Re-ID as a multiclassification problem of images, and proposed an ID Discriminative Embedding (IDE) network model, which treats each pedestrian as a different class and uses the pedestrian's ID as a classification label to train the deep neural network. Zheng et al. [55] and Chen et al. [3] jointly verification loss and ID loss can lead to better performance of CNN.

Different from the representation learning method, distance metric learning methods [5, 7, 11, 22, 26, 31, 32, 45] aim to learn a mapping from the original image to the feature embedding, so that the same pedestrian has a smaller distance in the feature space, and different person are farther away [29]. Triple loss is the most common distance metric learning method. Its principle is to define two images of the same person as a positive pair, while two images of different people are defined as a negative pair to guide the network model to training [47]. The traditional triple loss may have simple sample combinations and a lack of training for hard sample combinations. For this reason, some researchers consider improving the triple loss for mining hard samples [11, 31, 45]. Luo et al. [22] jointly trained the classification (ID) loss and the metric loss to accelerate the convergence of the model. However, the triple loss has a poor ability to constrain the samples within the class, while the center loss can shorten the distance of the samples within the class, and can effectively make up for this defect of triple loss. Therefore, we use classification loss, triple loss with hard sample mining, and center loss joint constraint model in our proposed method.

2.2. Local Features Alignments based Person Re-ID

Traditional global feature learning methods mainly focus on the appearance and spatial location information of pedestrians, but lack the learning of fine-grained local information. Recent works [2, 4, 10, 13, 17, 21, 25, 33, 34, 36, 39, 42, 49, 50] further improve the accuracy by learning deep local features. We have summarized three main approaches based on local feature learning: determining body parts according to pre-defined partitions, locating body parts through the joint point method, and locating local features through spatial attention. Some stripe-based methods [10, 34, 36, 39] divide the deep feature maps into regions according to certain predefined division rules to learn the local features. Li et al. [18] propose a Re-ID model with Part Prediction Alignment (PPA), which aims at aligning the predicted distributions between each part.

Ngo et al. [27, 28] explored the method of high-level feature extraction, and aim to explore context-based concept fusion by modeling inter-concept relationships, which are modeled not based on semantic reasoning. Semantic alignment-based person Re-ID has been investigated in a number of works [9, 12, 33, 49, 50, 58]. Some methods locate the key points of body parts to extract the body regions, and then use CNN to capture semantic features from different body regions to obtain discriminative local details information. In addition, some recent studies [2, 4, 17, 21] have introduced attention as a supplement to the discriminative features and achieved good performance.

However, the local feature learning method trend to learns the detailed information of a certain area of the pedestrian, but its reliability may be affected by pose changes and occlusions. In addition, most methods only focus on the parts with fixed semantics, cannot cover all the distinguishing information. Therefore, researchers often combine the methods of local and global feature learning [6, 33, 41, 44, 46, 48, 51] to enhance the final distinguishing feature representation. Wang et al. [41] proposed a feature learning strategy that combines global and local information, and designed a Multi-Granularity Network (MGN) to learn features of different granularities from pedestrian images. Wei et al. [44] proposed the Global-Local-Alignment Descriptor (GLAD), which learns the global and three local features separately, and finally connects them to form a distinctive and robust GLAD.

In general, the methods above either use hard alignment to match the local features or introduce additional supervision to assist the local alignment and seldom pay attention to the dynamic alignment of local features. In this paper, we combine the global features of pedestrians and the local features of horizontal stripe partitions and use a simple and efficient local sliding alignment strategy to dynamically align the local features.

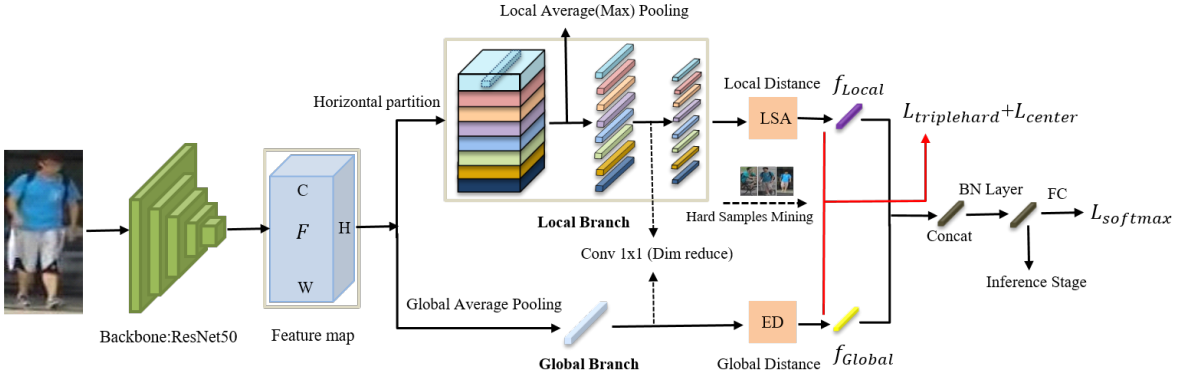


Fig. 2: The network structure of GLDFA-Net. After the input image passes through the stacked convolutional layers of the Resnet50 backbone network, the global branch and the local branch share the feature map. For global features, we can directly perform global average pooling on the feature map and use Euclidean Distance (ED) to calculate the global distance. For local features, we first partition the feature map horizontally, and obtain the feature vector of each horizontal strip through local average pooling. Then we use LSA to calculate the local alignment distance, and combine the global distance for triple loss with hard sample mining. Finally, we combine global features and local features as the final feature representation, and pass through a fully connected (FC) layer and a Softmax layer to achieve image classification.

Table 1

Comparison of component settings in GLDFA-Net. The size of the input image is set to 384×128 . "Component" represents the name of the branch. "Map Size" refers to the size of the output feature of each branch. "Dimension" represents the dimension of the output feature map. "Description" represents the symbol of the output feature.

Component	Map Size	Dimension	Description
Backbone	12×4	2048	Null
Global-branch	24×8	256	f_{Global}
Local-branch	24×8	256×8	$f_{Local}^i _{i=1}^8$

3. Methods

In this section, we first describe the network structure of GLDFA-Net, then introduce the local sliding alignment strategy, and finally we design the loss function of the model proposed in this paper.

3.1. Network Architecture

In order to allow CNN to learn more discriminative features, we design a novel GLDFA-Net framework for person Re-ID tasks. Figure 2 shows the architecture of our proposed network. We use Resnet50, which has competitive performance and relatively simple architecture, as the backbone network to extract feature maps of pedestrians [1, 24, 36]. We first remove the average pooling layer and subsequent layers of Resnet50, and then divide the part after the ResBlock4 block into two independent branches, naming them Global Branch and Local Branch, respectively. For the global branch, we use Global Average Pooling (GMP) to convert the feature maps into a global feature vector, and use 1×1 convolutional layer batch normalization and ReLU to reduce the 2048-dim feature to 256-dim. We change the step of the last spatial down-sampling of the Resnet50 backbone network from 2 to 1. When an image of size 384×128 is input, a feature map with a larger spatial size (24×8) can be obtained. Table 1 shows some details. For the local branch, we use horizontal average(max) pooling to evenly divide the output feature map into k strips in the horizontal direction, and average all column vectors in the same strip into a single column vector $l_i (i = 1, 2, 3, \dots, k)$, inspired by PCB [36], where the size of k is set to 8, and the dimension of l_i is set to 256. We learn local features independently on these strips.

In the testing phase, we reduce the global and local features to 256-dim and connected them to the final feature. In addition, the global branch and the local branch don't share weights, that is, their corresponding triple loss and classification loss are trained with independent weight constraints.

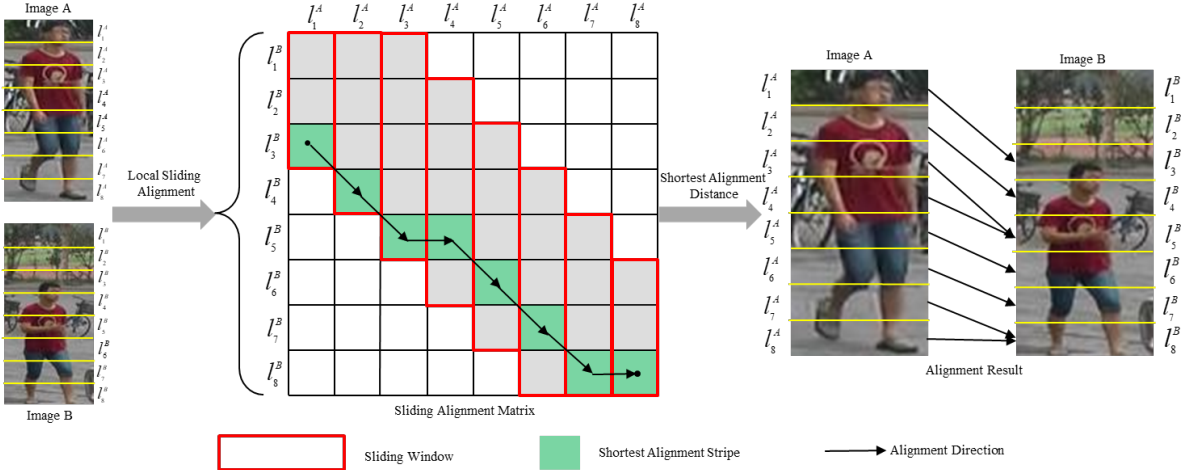


Fig. 3: Schematic diagram of the Local Sliding Alignment (LSA). First, we divide horizontal strips for pedestrians. Then, we set a sliding window for the partial strips from top to bottom. Finally, we calculate the shortest alignment distance from the horizontal strip in the window. The arrow direction represents the matching local feature, the solid arrow represents the shortest alignment distance, the dashed line represents the non-shortest alignment distance, and the alignment distance of the two images is the sum of the alignment distances of all local strips.

3.2. Local Sliding Alignment

In the training phase, we calculate the global distance of the global branch and the local distance of the local branch for the metric learning of the triple loss. In the inference stage, we use the local distance to calculate the similarity between the images. In this paper, we all use Euclidean distance to calculate the distance between the global branch and the local branch. We use f_G^A and f_G^B to represent the global features of images, respectively, and the Euclidean distance of the global feature can be expressed as:

$$G_{dis} = \|f_G^A - f_G^B\|_2 \quad (1)$$

We propose a dynamic alignment strategy called Local Sliding Alignment (LSA) to calculate local distance. The reason is that most traditional methods either use local hard alignment, or introduce the key points of the pedestrian's body structure to assist the pedestrian's local alignment to calculate the local distance. However, when there are wrong boundary detection frames and occlusions of pedestrians, the local hard alignment method is less effective for mining hard samples, and the key point-based method needs to introduce additional computing resources.

LSA is a combination of dynamic programming and sliding window, and its core idea is to first divide the local branching feature map into horizontal stripes, then set sliding windows for the horizontal stripes (where each sliding window is interrelated), and finally solve the local shortest alignment distance in the sliding window to obtain the global shortest alignment distance of the whole feature map. The details of the LSA is expressed in Algorithm 1, and Figure 3 shows a schematic representation of the process of its implementation. We divide horizontal strips for pedestrians, use $f_L^A = \{l_A^1, l_A^2, l_A^3, \dots, l_A^k\}$ and $f_L^B = \{l_B^1, l_B^2, l_B^3, \dots, l_B^k\}$ to represent the local features of images A and B respectively.

We set the sliding window for the horizontal stripe of the local branch. In real-world applications, we would recommend setting the size of the sliding window to be half the number of stripes, denoted as $W = k/2$, and the sliding step size S is set to 1 by default. The actual window size w_i corresponding to each stripe can be expressed as:

$$w_i = [\max(0, i - W/2), \min(k, i + W/2)] \quad (2)$$

where i takes the value of $1 \leq i \leq k$, k represents the number of horizontal stripes, inspired by PCB [36], where the value of k is 8 in this paper. The set of sliding windows of image A matching image B can be represented as $W_L^{AB} = \{w_1^A, w_2^A, w_3^A, \dots, w_k^A\}$. The set of sliding windows of image B matching image A can be represented as $W_L^{BA} = \{w_1^B, w_2^B, w_3^B, \dots, w_k^B\}$. We denote the shortest distance between the i -th stripe of image A and the sliding window of image B as d_i^{AB} , and the shortest distance between the i -th stripe of image B and the sliding window of

Algorithm 1 Local Sliding Alignment

Input: Images A B , sliding window W
Output: Align distance L^{dis}

```

1: Initialization:  $f_L^A = \{l_1^A, l_2^A, l_3^A, \dots, l_k^A\}, D_A = \emptyset$ ,  

    $f_L^B = \{l_1^B, l_2^B, l_3^B, \dots, l_k^B\}, D_B = \emptyset, count = 0$ 
2: while  $True$  do
3:   for  $each i$  do
4:      $d_{align} \leftarrow dis(l_i^A, l_i^B)$ 
5:      $w_{up} \leftarrow max(0, i - W/2)$ 
6:      $w_{down} \leftarrow min(k, i + W/2)$ 
7:     for  $j \leftarrow 1$  to  $k$  do
8:       if  $j \geq w_{up}$  and  $j \leq w_{down}$  then
9:          $d_{align} \leftarrow min(dis(l_i^A, l_j^B), d_{align})$ 
10:      end if
11:    end for
12:     $D_A \leftarrow d_{align}$ 
13:  end for
14:  if  $count > 0$  then
15:     $L^{dis} \leftarrow min(sum(D_A), sum(D_B))$ 
16:    break
17:  else
18:     $f_L^A \leftrightarrow f_L^B$ 
19:     $D_B \leftarrow D_A$ 
20:     $count \leftarrow count + 1$ 
21:  end if
22: end while
23: return  $L^{dis}$ 

```

image A as d_i^{BA} , then d_i^{AB} and d_i^{BA} can be expressed as:

$$d_i^{AB} = \min \left\{ \left\| l_i^A - l_i^B \right\|_2 \mid l_i^A \in f_L^A, l_i^B \in w_i^B \right\} \quad (3)$$

$$d_i^{BA} = \min \left\{ \left\| l_i^B - l_i^A \right\|_2 \mid l_i^B \in f_L^B, l_i^A \in w_i^A \right\} \quad (4)$$

We add the shortest alignment distance of each stripe of images A and B to the sets D_A and D_B respectively, $D_A = \{d_1^{AB}, d_2^{AB}, d_3^{AB}, \dots, d_k^{AB}\}$ and $D_B = \{d_1^{BA}, d_2^{BA}, d_3^{BA}, \dots, d_k^{BA}\}$. Then we get the shortest alignment distances L^{dis} of images A and B are obtained, then L^{dis} can be expressed as:

$$L_{dis} = \min \left(\sum_{i=1}^k d_i^{AB}, \sum_{i=1}^k d_i^{BA} \right) \quad (5)$$

In the training phase, we use LSA to calculate the local alignment distances and combine them with the global distances, together as the sample distance for triplet loss. LSA can shorten the distance of samples with the same ID, thus effectively mining hard samples and guiding the model to learn more discriminative features. In the inference phase, we calculate the distance between the two images as the sum of the global distance and the local distance for similarity measurement, which can further improve the accuracy of person matching. As shown in Figure 4, we get the local distance calculated by the local hard alignment method and the local sliding alignment (LSA) method respectively. Compared with the hard alignment strategy, the LSA we proposed can get a shorter alignment distance, which can make the distance among samples with the same ID shorter.

3.3. Loss Functions

In order to improve the model's ability to learn discriminative features, we joint classification loss and triplet loss to constrain the model. The classification loss usually connects a Fully Connected Layers (FC) for classification at the

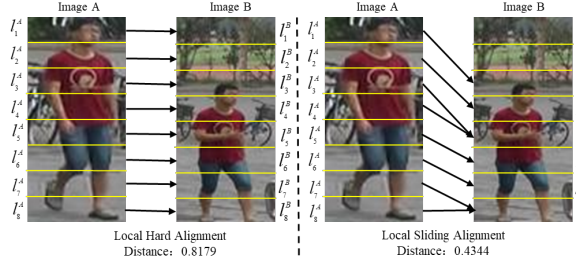


Fig. 4: Compare the local distance calculated by local hard alignment and local sliding alignment (LSA). The local distance obtained by using LSA is much shorter than the local distance calculated by local hard alignment.

end of the network, and maps the feature vector of the picture to the probability space through the Softmax activation function. Therefore, the cross-entropy loss for multiple classifications of person Re-ID can be expressed as:

$$\mathcal{L}_{id} = \sum_{i=1}^K q(x_i) \log p(y_i|x_i) \quad (6)$$

where K represents the number of ID categories of each batch of training samples, $q(x_i)$ represents the label of the sample image x_i , if x_i is identified as y_i , then $q(x_i) = 1$, otherwise $q(x_i) = 0$. $p(y_i|x_i)$ is the probability that the image x_i is predicted to be the category y_i using the Softmax activation function.

In order for the model to mine hard samples efficiently, We introduce an adaptive hard sample mining triplet loss (Triplethard) proposed by [31], which is an improved version of the original triplet loss. The loss function can be expressed as:

$$\mathcal{L}_{triplehard} = [m + w_p d(x_a, x_p) - w_n d(x_a, x_n)]_+ \quad (7)$$

$$w_p = \frac{\exp(d(x_a, x_p))}{\sum_{x \in P(a)} \exp(d(x_a, x))}, \quad (8)$$

$$w_n = \frac{\exp(-d(x_a, x_n))}{\sum_{x \in N(a)} \exp(d(x_a, x))}.$$

where $[\bullet]_+ = \max(0, \bullet)$, x_a is an anchor sample (Anchor), x_p is a positive sample (Positive), x_n is a negative sample (Negative), x_a and x_p have the same ID, x_a and x_n have different IDs, and m is a hyper parameter set manually. By training the model, the distance between x_a and x_p in Euclidean space is closer than the distance between x_a and x_n . We use the Softmax function to adaptively assign weights w_p and w_n to positive and negative samples, respectively.

Although the triple loss can effectively improve the spatial distribution of features, it has a poor ability to constrain samples within the class. However, the center loss can minimize the distance of samples within a class and improve the compactness of samples of the same class. Therefore, we introduce a joint constrained model of the center loss and the Triplethard loss to train. The center loss can be expressed as:

$$\mathcal{L}_{center} = \frac{1}{2} \sum_{i=1}^k \|f_{t_i} - c_{y_i}\|_2^2 \quad (9)$$

where k represents the number of ID categories of each batch of training samples, y_i is the label of the batch training sample image i , and c_{y_i} represents the class center of the deep feature f_{t_i} .

In our experiments, we calculate the Triplethard loss and center loss of global branch and local branch respectively. Therefore, the final Triplethard loss and center loss can be expressed as:

$$\mathcal{L}'_{triplehard} = \mathcal{L}_{triplehard}^g + \mathcal{L}_{triplehard}^l \quad (10)$$

$$\mathcal{L}'_{center} = \mathcal{L}^g_{center} + \mathcal{L}^l_{center} \quad (11)$$

We connect the features f^g and f^l of the two branches as the final feature, which can be written as $f_{final} = [f^g \cdot f^l]$, where $[\cdot]$ means concatenation. Finally, we use f_{final} to calculate the multi-class cross-entropy loss \mathcal{L}_{id} . Therefore, the final total loss \mathcal{L}_{total} is a combination of the three losses and can be expressed as:

$$\mathcal{L}_{total} = \mathcal{L}_{id} + \mathcal{L}'_{triplehard} + \lambda \mathcal{L}'_{center} \quad (12)$$

We set the weight λ of the center loss to 0.05.

4. Experimental Results

4.1. Implementation

We adjust the size of all the images for training and testing to 384×128 . Our method is implemented on the basis of the open source person Re-ID benchmark [23]. We use weights which is pretrained on ImageNet [8] to initialize the model. In the training phase. Firstly, the pedestrian images are performed random horizontal flipping, random erasure and normalization to enhance the training data. Then, while training the network model, in order to use the Triplehard loss and center loss better, we set the batch size to 32, select P samples with different identities randomly in each batch, and select K images randomly for each identity from the training set. In our experiment, $P = 8$ and $K = 4$. The weights of the Triplehard loss for global and local branches are both set to 0.3. We choose Adam as the optimizer of the model. We set the size of Epochs to 300, where the learning rate is 3.5×10^{-3} for the first 100 Epochs, the learning rate is 3.5×10^{-4} between 100 and 200 Epochs, and drops to 3.5×10^{-5} after 200 Epochs, and the weight attenuation is set to 10^{-5} . In addition, label smoothing (LS) [37] is used to improve the performance of the model. In the inference phase, we connect the feature vectors of the global branch and the local branch to generate the final feature representation. We use open source re-ranking (RK) [57] technology to improve query results. Finally, our model is implemented on the PyTorch platform and uses an NVIDIA 2080Ti GPU. Our experiments on all datasets share the same experimental settings as above.

4.2. Datasets

In this part, we will introduce the person Re-ID dataset used in this paper. Since Market1501 [52], DukeMTMC-reID [56] and CUHK03 [15] are currently the mainstream datasets for person Re-ID tasks, we will evaluate the performance on these datasets.

Market-1501. Market-1501 is a large-scale person Re-ID data set released in 2015. This data set is collected by 5 high-resolution cameras and 1 low-resolution camera in front of the Tsinghua University supermarket. It contains a total of 32668 images of 1501 different pedestrians. The pedestrian detection box is marked by manual marking and automatic detector DPM.

DukeMTMC-reID. DukeMTMC-reID is a subset of the multi-camera multi-target tracking data set DukeMTMC [30], which is also a person Re-ID data set. The data set was collected by 8 static high-definition cameras on the campus of Duke University. It contains a total of 36,441 images of 1812 different pedestrians. The size of each image is variable, and the pedestrian detection frame is manually labeled.

CUHK03. CUHK03 is a large-scale person Re-ID dataset. Images in CUHK03 are captured by 10 cameras on the campus of the Chinese University of Hong Kong, including 1,360 different pedestrians, a total of 13,164 images, using manual marking and automatic detection to mark pedestrian detection frames. The CUHK03 data set is improved on the basis of the CUHK01 [14] and CUHK02 [16] data sets, increasing the number of cameras and collected images, so that images from more cameras can be captured.

Partial-Market and Partial-Duke. The person images in the above dataset are carefully processed and contain almost the complete body of a person with limited detection of bounding box errors, occlusions and pose changes of person. The person Re-ID task in this case is able to obtain a high performance. To better verify the performance advantage of our method in processing part of the person Re-ID, we apply random erase and random crop operations to Market-1501 and DukeMTMC-ReID, where some images are randomly erased 10%-30% in the vertical direction for modeling occlusion and some images are randomly cropped 20%-30% in the vertical direction for simulate detection of bounding box errors. We obtain the partial person Re-ID datasets Partial-Market and Partial-Duke. We also do ablation study on Partial-Market and Partial-Duke to verify the effectiveness of our method in solving partial person Re-ID.

Table 2

Ablation experiments on the Market1501 dataset. "TH" refers to the Triplehard loss. "G" refers to the use of only global feature learning network and Triplehard loss. "L" means that only the local feature learning combined network and Triplehard loss. "GL" refers to the use of global-local feature learning network and Triplehard loss. "LSA" refers to the use of a local sliding alignment strategy to match the local features.

Methods	mAP	R-1	R-5	R-10
ResNet50	70.6	83.7	92.8	96.3
ResNet101	73.4	85.3	93.0	97.2
ResNet50+TH	73.2	86.8	92.5	97.4
G(Global+TH)	77.6	89.7	93.4	97.5
L(Local+TH)	78.9	90.1	94.0	97.4
GL(Global-Local+TH)	80.5	90.4	94.6	98.0
L+LSA	80.7	92.3	95.3	98.2
GL+LSA	81.6	92.8	95.6	98.2
GLDFA-Net w/o TH	82.7	91.9	94.3	97.4
GLDFA-Net w/o LSA	84.2	92.6	95.0	97.8
GLDFA-Net	86.1	94.8	97.2	98.4

4.3. Ablation Study

In order to further study the effectiveness of global-local feature combination and Local Sliding Alignment (LSA) strategy in GLDFA-Net, we design several ablation experiments with different settings on the Market-1501 dataset. The remaining parameters for each comparison experiments are exactly the same as GLDFA-Net in Section 4.1. In addition, we use Resnet50 as a benchmark for comparing global and local feature networks, use Softmax as the classification loss function by default, and ensure that the selected model can get the best experimental performance under specified conditions. Table 2 shows the results of ablation experiments related to GLDFA-Net components but with different settings, from which we can get the following conclusions:

The impact of multiple networks: Usually the global branch network learns the coarse-grained global information of pedestrians. The local branch network learns the detailed information of the pedestrian part. We are convinced that combining global and local branches can achieve better performance. Therefore, we use Resnet50 as the benchmark network to separately train global branches, local branches and global-local networks, and use Softmax classification loss and Triplehard loss training models to explore the impact of different network structures on model performance. We can observe from Table 2 that the experimental results of the local branch network (Local + TH) are slightly better than the global branch network (Global + TH), and the global-local (Global-Local + TH) combined network is significantly better than the previous two. GLDFA-Net can achieve 92.6% Rank-1 accuracy and 84.2% mAP without using LSA (w/o LSA). Compared with the independent network, the global-local network can learn more discriminative features, because the global branch and the local branch will influence each other during the training process, so as to learn complementary global and local features as the distinguishing information of pedestrian identity.

The impact of local feature alignment: There are often challenges such as pedestrian bounding box errors, posture changes, and partial occlusion, which will limit the alignment of local features and affect the accuracy of person Re-ID. In order to verify the effectiveness of the Local Sliding Alignment (LSA) strategy for partial Re-ID, we conduct a comparative experiment on the Market1501 dataset. L+LSA refers to the combined training model using local branch and LSA, GL+LSA refers to the combined training model using global-local and LSA, and our loss function is set to a combination of Softmax classification loss and Triplehard loss. We compared the experimental results of L and GL in Table 2, and found that the accuracy of Rank-1 using LSA increased by 2.2% and 2.4%, and mAP increased by 1.8% and 1.1%, respectively. Our method GLDFA-Net can achieve the experimental performance of Rank-1/mAP=86.1%/94.8% when using LSA. Obviously, compared with local and global, LSA can greatly improve performance. LSA not only helps to mine samples in the training phase, but also helps to calculate the alignment distance between samples in the inference phase. In general, the LSA we proposed is very effective for some people's Re-ID tasks, and it is of great significance for studying large-scale person Re-ID tasks in real scenarios.

The impact of Triplehard loss: In the person Re-ID task, we use Softmax classification loss for representation learning, and Triplehard loss for metric learning. In order to verify the enhancement effect of the classification loss and Triplehard loss joint training on the model performance, we use the Resnet50 benchmark nework and GLDFA-Net to conduct experiments respectively. It is observed from the experimental results in Table 2 that after using Triplehard



Fig. 5: Sampled person images of Partial-Market

Table 3

Ablation study on Partial-Market and Partial-Duke.

Methods	Partail-Market		Partail-Duke	
	mAP	Rank-1	mAP	Rank-1
ResNet50	42.8	60.5	39.7	52.3
GLDFA-Net w/o TH	48.0	62.4	42.9	54.7
GLDFA-Net w/o LSA	50.1	67.4	44.2	57.5
GLDFA-Net	54.6	72.4	48.2	60.9

loss (TH), the Rank-1/mAP performance of the ResNet-50 baseline model is improved by 3.1%/2.6%, and the Rank-1/mAP performance of GLDFA-Net is improved by 3.9%/3.4%. But compared to the benchmark model, Triplehardt loss improves the performance of the GLDFA-Net model even more. Compared to using the Softmax classification loss only, Triplehardt loss can learn the mapping relationship from the original image to the embedding space, and can effectively improve the spatial distribution of features.

Evaluation on partial person Re-ID: We argue that the person images in Market-1501 and DukeMTMC-ReID are manually processed and contain almost the complete body of a person, with limited detection of bounding box errors, occlusions, and pose changes for pedestrians. To better evaluate the effectiveness of GLDFA-Net, we test our method on Partial-Market and Partial-Duke. Figure 5 shows some example images, which are partial person Re-ID images of Partial-Market.

To verify the effectiveness of GLDFA-Net in partial person Re-ID, we conducted ablation studies on Partial-Market and Partial-Duke, and the evaluation results are shown in Table 3. As a whole, the rank-1 accuracy and mAP of both baseline(Resnet50) and GLDFA-Net on Partial-Market and Partial-Duke decreased, where the rank-1 accuracy of baseline on Market1501 was 83.7%, but its performance on Partial-Market decreased to 60.5%. The rank-1 accuracy of GLDFA-Net is 94.8% and 90.1% for Market-1501 and DukeMTMC-ReID, respectively, but its performance drops to 72.4% and 60.9% for Partial-Market and Partial-Duke, respectively. The GLDFA-Net using LSA in the case of Partial-Market and Partial-Duke achieve 4.5% and 3.4% improvement in Rank-1 accuracy, respectively. In overview, our proposed GLDFA-Net is more effective for partial person Re-ID tasks, which is more suitable for large-scale person Re-ID in realistic scenarios.

4.4. Parameters Analysis

We analyze some important parameters of GLDFA-Net (and with LSA) introduced in Section 3.2 on Market-1501. Once optimized, the same parameters are used for all three datasets in the train and inference stage.

The impact of the number of stripes k : The number of stripes k determines the granularity of the local features. When $k = 1$, the features learned by the neural network are global features, and we usually assume that the retrieval accuracy of Re-ID increases as k increases. However, the retrieval accuracy does not necessarily increase all the time. We set the size of the sliding window to half of the number of stripes. As shown in Figure 6(a), the retrieval accuracy rank-1 and mAP increase with the number of stripes before $k = 8$. The alignment results for the different number of stripes are shown in Figure 7, where the alignment distance for $k = 8$ is smaller than that for $k = 6$. After $k = 8$, the retrieval accuracy rank-1 and mAP hardly fluctuate, probably because the sliding window W increases while the stripe number k increases, and the local feature alignment distance does not change much. In real-world applications,

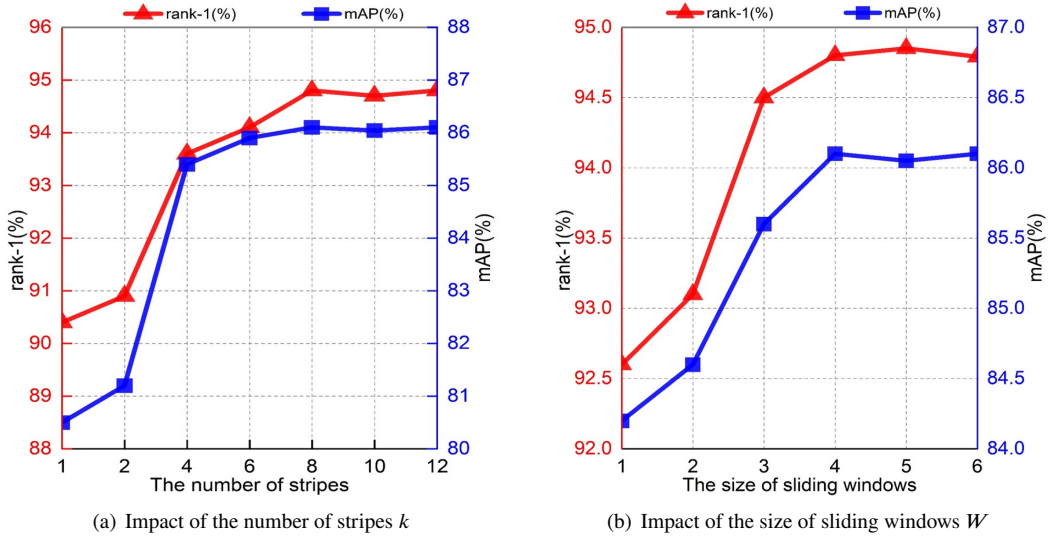


Fig. 6: Parameter analysis. (a):The impact of the number of stripes k . We set the size of the sliding window to be half the number of stripes. (b):The impact of the size of sliding windows W . We set the number of stripes is 8.

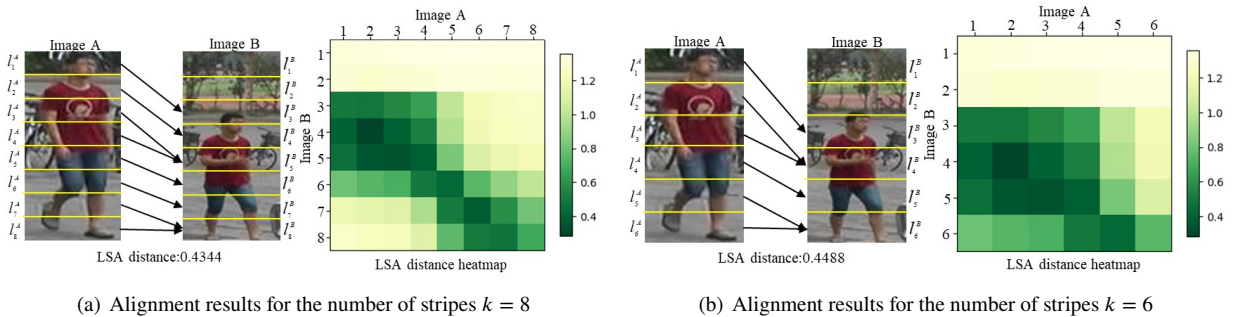


Fig. 7: Example alignment results for different number of stripes. (a): Alignment results for the number of stripes $k = 8$. (b) :Alignment results for the number of stripes $k = 6$. We also show the distance maps/matrices of the local features of the two images.

the increase in the number of stripes affects the execution efficiency of the model, and we suggest that the number of stripes $k = 8$.

The impact of the size of sliding windows W : In Figure 6(b), we set the number of stripes $k = 8$ and explore the effect of the size of the sliding window W on the retrieval accuracy. When $W = 1$, it is the traditional way of hard alignment of stripes. Before $W = 4$, the retrieval accuracy rank-1 and mAP increase with the increase of sliding window W , the reason is that as W increases, the stripes of one image can match more stripes within the sliding window of another image, thus getting a shorter alignment distance to improve the retrieval accuracy. After $W = 4$, the retrieval accuracy rank-1 and mAP hardly change, the reason may be that the shortest alignment distance within the window remains the same. In practical applications, we propose that $W = k/2$ can align almost most of the body parts.

4.5. Comparison with State-of-the-Art Methods

We compared GLDFA-Net with recent methods on the three data sets of Market1501, DukeMTMC-ReID and CUHK03 to prove that GLDFA-Net is superior to other existing methods. In order to better illustrate the comparison results on each data set, we will introduce the following in detail:



Fig. 8: Top-10 ranking list for some query images on Market-1501 datasets by GLDFA-Net. The first row shows the search results with posture changes, the second row shows the search results with incorrect bounding box detection, and the third row shows the search results with partial occlusion. The images with green borders belong to the same identity to the given query image, while the one with red border show the incorrect identity.

Market1501: Table 4 shows the person Re-ID results on Market1501. We divide these methods into two groups: global-based methods and local-based methods. From the overall experimental results, the performance of local-based methods is generally higher than that of methods with global features, such as SVDNet[35], Mancs[40], Triplet Loss[11]. For the local-based methods, in the single query mode, PCB+RPP[36] only uses the local horizontal stripe partition and Refined Part Pooling(RPP) to obtain better results, but this type of method often ignores the impact of global features on discriminative feature mining. We combine coarse-grained global features and fine-grained local features. Our GLDFA-Net achieves Rank-1/mAP=94.8%/86.1%, which improves the accuracy of Rank-1 by 1.0% and 4.5% on mAP compared to PCB+RPP. After using re-ranking, our experimental results can reach Rank-1/mAP=95.6%/93.5%, which is much better than other current methods. On the one hand, we use a combination of global and local features to enrich the discriminative features of pedestrians, which helps to improve the accuracy of the model. On the other hand, although RPP obtains local discriminative features by refined pooling of local stripes, it still belongs to the category of hard alignment, which is less effective than GLDFA-Net in mining hard samples in the case of bounding box detection error or partial occlusion. Figure 8 shows the top-10 ranking list of GLDFA-Net query images on the Market-1501 dataset. These retrieved images are all from the Gallery collection and captured by different cameras. The first row of pedestrians has a large variation of posture or gait, our method can still get all the correct retrieval results by aligning the invariant features of the body parts. Errors in the pedestrian boundary detection box in the second row lead to easy lose important information or introduce background information, which our method can effectively mitigate by dynamically aligning the pedestrian body parts. The third row shows the retrieval results for partially occluded pedestrians. Although the occluded area not only loses a lot of important information but also introduces additional noise, our alignment method is still able to obtain high retrieval results. The retrieval results show strong robustness, except for the last matching error in the second row. We attribute this surprising result to the effect of dynamic alignment of local features that reflect the robustness of their identity.

DukeMTMC-ReID: As can be seen from Table 4, GLDFA-Net also shows better performance on the more challenging DukeMTMC-reID dataset. Without re-ranking, our method can achieve an accuracy of Rank-1/mAP =87.5% /76.9%. As a comparison, AlignedReID++[24] has a similar structure to our method, but our method improves Rank-1 by 5.4% and mAP by 7.2%. The reason is that LSA aligns the local features adaptively, so it can effectively mine hard samples and metric similarity. The reason is that AlignedReID++ aligns local stripes using a complete alignment strategy, and when there is an error in the detection of the bounding box, the wrong stripes matching result will also be calculated into the alignment distance, thus affecting the final similarity. LSA introduces the ideas of sliding window

Table 4

Comparison with the state-of-the-art methods in terms of Rank-1 and mAP on the Market-1501, DukeMTMC-reID and CUHK03 datasets. Group 1: the methods only using global features. Group 2: the methods using local features. The bold font represents the best result. RK stands for the method of using re-ranking [57]

Methods	Reference	Market-4501		DukeMTMC-reID		CUHK03			
		mAP	Rank-1	mAP	Rank-1	mAP	Rank-1	mAP	Rank-1
Triplet Loss[11]	arXiv'17	69.1	84.9	58.8	76.7	-	-	-	-
SVDNet[35]	ICCV'17	62.1	82.3	71.8	84.9	37.3	41.5	37.8	40.9
* Mancs[40]	ECCV'18	82.3	93.1	76.4	86.4	60.5	65.5	63.9	69.0
§ PDC[33]	ICCV'17	63.4	84.1	-	-	-	-	-	-
§ GLAD[44]	TM'19	73.9	89.9	-	-	-	-	-	-
* HA-CNN[17]	CVPR'18	75.5	91.2	63.8	80.5	38.6	41.7	41.0	44.4
§ Pose-transfer[20]	CVPR'18	56.9	78.5	48.1	68.6	38.7	71.6	42.0	-
† PCB[36]	ECCV'18	77.4	92.3	66.1	81.8	54.2	61.3	-	-
† PCB+RPP[36]	ECCV'18	81.6	93.8	69.2	83.3	57.5	63.7	-	-
† HPM[10]	AAAI'18	82.7	94.2	74.3	86.6	57.5	63.9	-	-
† MGN[19]	ACCV'19	-	-	-	-	66.0	68.0	67.4	68.0
* MHN(IDE)[2]	ICCV'19	83.6	93.6	75.2	87.5	61.2	67.0	65.1	69.7
† * VPM[34]	CVPR'19	80.8	93.0	72.6	83.6	-	-	-	-
* PL-Net[46]	TIP'19	69.3	88.2	-	-	-	-	-	-
† * AANet[38]	CVPR'19	83.4	93.9	74.3	87.6	-	-	-	-
† AlignedReID++[24]	PR'19	79.1	91.8	69.7	82.1	59.6	61.5	-	-
* DHA[43]	TIP'20	76.0	91.3	64.1	84.3	-	-	-	-
§ PPA+TS[18]	CVIU'21	79.6	92.4	71.8	85.1	62.0	64.6	66.3	69.2
§ MBRAN[9]	ICMM'20	83.8	94.6	76.9	87.1	-	-	-	-
§ * FGSAM [58]	TIP'20	85.4	91.6	71.4	85.9	-	-	-	-
GLDFA-Net		86.1	94.8	76.9	87.5	68.4	72.3	68.9	73.1
GLDFA-Net(RK)		93.5	95.6	89.5	90.1	70.3	73.6	72.1	76.5

† Stripes related, * Attention related, § Pose or human parsing related.

and dynamic programming, and by adaptively aligning the local features of pedestrians, it can effectively mine the hard samples and the similarity metric is performed.

CUHK03: As shown in Table 4, GLDFA-Net reached Rank-1/mAP = 73.1%/68.9% on the manually labeled CUHK03 dataset. In particular, Rank-1/mAP = 72.3%/68.4% is achieved on the automatically detected CUHK03 dataset, which has exceeded the experimental results of most published methods. Although the automatically detected CUHK03 dataset is prone to incorrect pedestrian bounding boxes, which will produce missing or redundant information of body parts, our method uses dynamic alignment of the local features, which can effectively avoid the influence of these factors and can produce advanced accuracy.

5. Conclusion

In this paper, we construct a global-local dynamic feature alignment network based framework, GLDFA-Net for the person Re-ID task. We first propose LSA, a simple and efficient local sliding feature alignment strategy that can dynamically align local features of pedestrians by setting sliding windows on their local stripes. LSA can effectively suppress spatially misalignment and the noises from unshared regions, and does not require the introduction of additional auxiliary pose information. Then, we introduce LSA into the local branch of GLDFA-Net for guiding the computation of distance metric, which can further improve the performance of the model. Evaluation experiments on the Market-1501, DukeMTMC-reID and CUHK03 datasets clearly show that the proposed GLMG-Net has reached the latest experimental performance on multiple benchmark datasets. In the future, we will introduce knowledge distillation and transfer learning technologies to extend GLDFA-Net to cross-domain person Re-ID tasks.

CRediT authorship contribution statement

Zhangqiang Ming: Conceptualization, Methodology, Software, Investigation, Writing-original draft, Revision. **Yong Yang:** Data Curation, Visualization, Validation. **Xiaoyong Wei:** Writing-Review, Funding Acquisition. **Jianrong Yan:** Data curation, Visualization, Investigation. **Xiangkun Wang:** Writing-Review, Data curation. **Fengjie Wang:** Writing-Review, Visualization, Investigation. **Min Zhu:** Conceptualization, Writing - Review & Editing, Supervision, Resources.

Declaration of Competing Interest

The authors declare that they have no known competing financial interests or personal relationships that could have appeared to influence the work reported in this paper.

References

- [1] Bai, X., Yang, M., Huang, T., Dou, Z., Yu, R., Xu, Y., 2020. Deep-person: Learning discriminative deep features for person re-identification. *Pattern Recognition* 98, 107036.
- [2] Chen, B., Deng, W., Hu, J., 2019a. Mixed high-order attention network for person re-identification. *Proceedings of the IEEE International Conference on Computer Vision* , 371–381.
- [3] Chen, H., Wang, Y., Shi, Y., Yan, K., Geng, M., Tian, Y., Xiang, T., 2018. Deep transfer learning for person re-identification. *2018 IEEE Fourth International Conference on Multimedia Big Data (BigMM)* , 1–5.
- [4] Chen, T., Ding, S., Xie, J., Yuan, Y., Chen, W., Yang, Y., Wang, Z., 2019b. Abd-net: Attentive but diverse person re-identification. *Proceedings of the IEEE/CVF International Conference on Computer Vision* , 8350–8360.
- [5] Chen, W., Chen, X., Zhang, J., Huang, K., 2017. Beyond triplet loss: A deep quadruplet network for person re-identification. *2017 IEEE Conference on Computer Vision and Pattern Recognition (CVPR)* , 403–412.
- [6] Chen, X., Fu, C., Zhao, Y., Zheng, F., Song, J., Ji, R., Yang, Y., 2020. Salience-guided cascaded suppression network for person re-identification. *Proceedings of the IEEE Conference on Computer Vision and Pattern Recognition (CVPR)* , 3297–3307.
- [7] Cheng, D., Gong, Y., Zhou, S., Wang, J., Zheng, N., 2016. Person re-identification by multi-channel parts-based cnn with improved triplet loss function. *Proceedings of the IEEE Conference on Computer Vision and Pattern Recognition (CVPR)* , 1335–1344.
- [8] Deng, J., Dong, W., Socher, R., Li, L.J., Li, K., Fei-Fei, L., 2009. Imagenet: A large-scale hierarchical image database. *Proceedings of the IEEE Conference on Computer Vision and Pattern Recognition* , 248–255.
- [9] Fang, H., Chen, J., Tian, Q., 2020. Multi-branch body region alignment network for person re-identification. *International Conference on Multimedia Modeling* , 341–352.
- [10] Fu, Y., Wei, Y., Zhou, Y., Shi, H., Huang, G., Wang, X., Yao, Z., Huang, T., 2018. Horizontal pyramid matching for person re-identification. *Proceedings of the AAAI conference on artificial intelligence* .
- [11] Hermans, A., Beyer, L., Leibe, B., 2017. In defense of the triplet loss for person re-identification. *arXiv preprint arXiv:1703.07737* abs/1703.07737v2.
- [12] Jin, X., Lan, C., Zeng, W., Wei, G., Chen, Z., 2020. Semantics-aligned representation learning for person re-identification. *Proceedings of the AAAI Conference on Artificial Intelligence* 34, 11173–11180.
- [13] Kalayeh, M.M., Basaran, E., Gökmen, M., Kamasak, M.E., Shah, M., 2018. Human semantic parsing for person re-identification. *Proceedings of the IEEE Conference on Computer Vision and Pattern Recognition* , 1062–1071.
- [14] Li, W., Wang, X., 2013. Locally aligned feature transforms across views. *Proceedings of the IEEE Conference on Computer Vision and Pattern Recognition* , 3594–3601.
- [15] Li, W., Zhao, R., Wang, X., 2013. Human reidentification with transferred metric learning. *Asian Conference on Computer Vision* , 31–44.
- [16] Li, W., Zhao, R., Xiao, T., Wang, X., 2014. Deepreid: Deep filter pairing neural network for person re-identification. *Proceedings of the IEEE Conference on Computer Vision and Pattern Recognition* , 152–159.
- [17] Li, W., Zhu, X., Gong, S., 2018. Harmonious attention network for person re-identification. *Proceedings of the IEEE Conference on Computer Vision and Pattern Recognition* , 2285–2294.
- [18] Li, Z., Lv, J., Chen, Y., Yuan, J., 2021. Person re-identification with part prediction alignment. *Computer Vision and Image Understanding* 205, 103172.
- [19] Lin, Y., Zheng, L., Zheng, Z., Wu, Y., Hu, Z., Yan, C., Yang, Y., 2019. Improving person re-identification by attribute and identity learning. *Asian Conference on Computer Vision* 95, 151–161.
- [20] Liu, J., Ni, B., Yan, Y., Zhou, P., Cheng, S., Hu, J., 2018. Pose transferrable person re-identification. *2018 IEEE/CVF Conference on Computer Vision and Pattern Recognition* , 4099–4108.
- [21] Liu, X., Zhao, H., Tian, M., Sheng, L., Shao, J., Yi, S., Wang, X., 2017. Hydraplus-net: Attentive deep features for pedestrian analysis. *Proceedings of the IEEE international conference on computer vision* , 350–359.
- [22] Luo, H., Gu, Y., Liao, X., Lai, S., Jiang, W., 2019a. Bag of tricks and a strong baseline for deep person re-identification. *Proceedings of the IEEE Conference on Computer Vision and Pattern Recognition Workshops (CVPRW)* , 1487–1495.
- [23] Luo, H., Jiang, W., Gu, Y., Liu, F., Liao, X., Lai, S., Gu, J., 2020. A strong baseline and batch normalization neck for deep person re-identification. *IEEE Transactions on Multimedia* 22, 2597–2609.
- [24] Luo, H., Jiang, W., Zhang, X., Fan, X., Qian, J., Zhang, C., 2019b. Alignedreid++: Dynamically matching local information for person re-identification. *Pattern Recognition* 94, 53–61.

[25] Miao, J., Wu, Y., Liu, P., Ding, Y., Yang, Y., 2019. Pose-guided feature alignment for occluded person re-identification. Proceedings of the IEEE International Conference on Computer Vision (ICCV) , 542–551.

[26] Mishchuk, A., Mishkin, D., Radenovic, F., Matas, J., 2017. Working hard to know your neighbor's margins: Local descriptor learning loss. Proceedings of the 31st International Conference on Neural Information Processing Systems , 4829–4840.

[27] Ngo, C.W., Jiang, Y.G., Wei, X.Y., Zhao, W., Wang, F., Wu, X., Tan, H.K., 2008. Beyond semantic search: What you observe may not be what you think. trecvid workshop .

[28] Ngo, C.W., Pan, Z., Wei, X., Wu, X., Tan, H.K., Zhao, W., 2005. Motion driven approaches to shot boundary detection, low-level feature extraction and bhc rushes characterization at trecvid 2005. trecvid workshop .

[29] Oh Song, H., Xiang, Y., Jegelka, S., Savarese, S., 2016. Deep metric learning via lifted structured feature embedding. Proceedings of the IEEE Conference on Computer Vision and Pattern Recognition (CVPR) , 4004–4012.

[30] Ristani, E., Solera, F., Zou, R., Cucchiara, R., Tomasi, C., 2016. Performance measures and a data set for multi target multi camera tracking. European conference on computer vision , 17–35.

[31] Ristani, E., Tomasi, C., 2018. Features for multi-target multi-camera tracking and re-identification. Proceedings of the IEEE Conference on Computer Vision and Pattern Recognition , 6036–6046.

[32] Shi, H., Yang, Y., Zhu, X., Liao, S., Lei, Z., Zheng, W., Li, S.Z., 2016. Embedding deep metric for person re-identification: A study against large variations. In European Conference on Computer Vision , 732–748.

[33] Su, C., Li, J., Zhang, S., Xing, J., Gao, W., Tian, Q., 2017. Pose-driven deep convolutional model for person re-identification. Proceedings of the IEEE International Conference on Computer Vision (ICCV) , 3980–3989.

[34] Sun, Y., Xu, Q., Li, Y., Zhang, C., Li, Y., Wang, S., Sun, J., 2019. Perceive where to focus: Learning visibility-aware part-level features for partial person re-identification. Proceedings of the IEEE/CVF Conference on Computer Vision and Pattern Recognition , 393–402.

[35] Sun, Y., Zheng, L., Deng, W., Wang, S., 2017. Svdnet for pedestrian retrieval. Proceedings of the IEEE International Conference on Computer Vision (ICCV) , 3820–3828.

[36] Sun, Y., Zheng, L., Yang, Y., Tian, Q., Wang, S., 2018. Beyond part models: Person retrieval with refined part pooling (and a strong convolutional baseline). Proceedings of the European conference on computer vision (ECCV) , 480–496.

[37] Szegedy, C., Vanhoucke, V., Ioffe, S., Shlens, J., Wojna, Z., 2016. Rethinking the inception architecture for computer vision. Proceedings of the IEEE Conference on Computer Vision and Pattern Recognition (CVPR) , 2818–2826.

[38] Tay, C.P., Roy, S., Yap, K.H., 2019. Aanet: Attribute attention network for person re-identifications. Proceedings of the IEEE Conference on Computer Vision and Pattern Recognition (CVPR) , 7127–7136doi:10.1109/CVPR.2019.00730.

[39] Varior, R.R., Shuai, B., Lu, J., Xu, D., Wang, G., 2016. A siamese long short-term memory architecture for human re-identification. European conference on computer vision , 135–153.

[40] Wang, C., Zhang, Q., Huang, C., Liu, W., Wang, X., 2018a. Mancs: A multi-task attentional network with curriculum sampling for person re-identification. Computer Vision ECCV 2018 , 384–400.

[41] Wang, G., Yuan, Y., Chen, X., Li, J., Zhou, X., 2018b. Learning discriminative features with multiple granularities for person re-identification .

[42] Wang, P., Zhao, Z., Su, F., Zu, X., Boulgouris, N.V., 2021. Horeid: Deep high-order mapping enhances pose alignment for person re-identification. IEEE Transactions on Image Processing 30, 2908–2922.

[43] Wang, Z., Jiang, J., Wu, Y., Ye, M., Bai, X., Satoh, S.I., 2020. Learning sparse and identity-preserved hidden attributes for person re-identification. IEEE Transactions on Image Processing 29, 2013–2025.

[44] Wei, L., Zhang, S., Yao, H., Gao, W., Tian, Q., 2019. Glad: Global-local-alignment descriptor for scalable person re-identification. IEEE Transactions on Multimedia 21, 986–999.

[45] Xiao, Q., Luo, H., Zhang, C., 2017. Margin sample mining loss: A deep learning based method for person re-identification. arXiv preprint arXiv:1710.00478 .

[46] Yao, H., Zhang, S., Hong, R., Zhang, Y., Xu, C., Tian, Q., 2019. Deep representation learning with part loss for person re-identification. IEEE Transactions on Image Processing 28, 2860–2871.

[47] Ye, M., Shen, J., Lin, G., Xiang, T., Shao, L., Hoi, S.C., 2021. Deep learning for person re-identification: A survey and outlook. IEEE Transactions on Pattern Analysis and Machine Intelligence .

[48] Zhang, Z., Lan, C., Zeng, W., Jin, X., Chen, Z., 2020. Relation-aware global attention for person re-identification. Proceedings of the IEEE Conference on Computer Vision and Pattern Recognition (CVPR) .

[49] Zhao, H., Tian, M., Sun, S., Shao, J., Yan, J., Yi, S., Tang, X., 2017a. Spindle net: Person re-identification with human body region guided feature decomposition and fusion. Proceedings of the IEEE Conference on Computer Vision and Pattern Recognition (CVPR) , 1077–1085.

[50] Zhao, L., Li, X., Zhuang, Y., Wang, J., 2017b. Deeply-learned part-aligned representations for person re-identification. Proceedings of the IEEE International Conference on Computer Vision (ICCV) , 3239–3248.

[51] Zheng, F., Deng, C., Sun, X., Jiang, X., Guo, X., Yu, Z., Ji, R., 2019. Pyramidal person re-identification via multi-loss dynamic training. Proceedings of the IEEE Conference on Computer Vision and Pattern Recognition (CVPR) , 8506–8514.

[52] Zheng, L., Shen, L., Tian, L., Wang, S., Wang, J., Tian, Q., 2015. Scalable person re-identification: A benchmark. Proceedings of the IEEE International Conference on Computer Vision (ICCV) , 1116–1124.

[53] Zheng, L., Yang, Y., Hauptmann, A.G., 2016. Person re-identification: Past, present and future. arXiv preprint arXiv:1610.02984 abs/1610.02984v1.

[54] Zheng, L., Zhang, H., Sun, S., Chandraker, M., Yang, Y., Tian, Q., 2017a. Person re-identification in the wild. Proceedings of the IEEE Conference on Computer Vision and Pattern Recognition (CVPR) , 1367–1376.

[55] Zheng, Z., Zheng, L., Yang, Y., 2017b. A discriminatively learned cnn embedding for person reidentification. ACM Transactions on Multimedia Computing, Communications, and Applications 14, 1–20.

- [56] Zheng, Z., Zheng, L., Yang, Y., 2017c. Unlabeled samples generated by gan improve the person re-identification baseline in vitro. Proceedings of the IEEE International Conference on Computer Vision (ICCV) , 3774–3782.
- [57] Zhong, Z., Zheng, L., Cao, D. and Li, S., 2017. Re-ranking person re-identification with k-reciprocal encoding. Proceedings of the IEEE Conference on Computer Vision and Pattern Recognition (CVPR) , 3652–3661.
- [58] Zhou, Q., Zhong, B., Lan, X., Sun, G., Zhang, Y., Zhang, B., Ji, R., 2020. Fine-grained spatial alignment model for person re-identification with focal triplet loss. IEEE Transactions on Image Processing 29, 7578–7589.